Vacancy-solute clustering in Fe-Cr alloys after neutron irradiation

Konstantinovic, M. J.; Ulbricht, A.; Brodziansky, T.; Castina, N.; Malerba, L.;

Originally published:

July 2020

Journal of Nuclear Materials 540(2020), 152341

DOI: https://doi.org/10.1016/j.jnucmat.2020.152341

Vacancy-solute clustering in Fe-Cr alloys after neutron irradiation

M.J. Konstantinović[a,*], A. Ulbricht[b], T. Brodziansky[d], N. Castin[a], L. Malerba[d]

[a] *Studiecentrum voor Kernenergie/Centre d'Etude de l'Energie Nucléaire (SCK CEN), Boeretang 200, B-2400 Mol, Belgium*
[b] *Helmholtz-Zentrum Dresden-Rossendorf (HZDR), Bautzner Landstraße 400, 01328 Dresden, Germany*
[c] *Faculty of electrical engineering and information technology, Slovak University of Technology in Bratislava, Vazovova 5, 811 07 Bratislava, Slovakia*
[d] *Division of Energy Materials, CIEMAT, Avenida Complutense 40, 28040 Madrid, Spain*

Abstract

Vacancy-solute clustering in neutron irradiated Fe-Cr alloys with various concentrations of Cr and minor solutes (Ni, Si and P) were studied by using coincidence Doppler broadening spectroscopy and small angle neutron scattering techniques. The results from both experiments, supported by an object kinetic Monte Carlo model, show in a very consistent way the existence and formation of vacancy-CrNiSiP clusters that play detrimental role in irradiation hardening. Similar solute cluster number density of about 30 to 50 $\times 10^{16} cm^{-3}$ and an average diameter of about 1 nm were estimated for all alloys containing minor solutes, irrespectively of the chromium content. In Fe9Cr ferritic and Fe9Cr ferritic/martensitic alloys, with significantly reduced concentration of minor solute elements, the main defects are vacancy clusters, with an average cluster size size of about 10 and 2 vacancies, respectively. Large concentration of α'-precipitates was observed in Fe14Cr(NiSiP). However, both vacancy clusters and α'-precipitates provide significantly less impact to hardening in comparison to vacancy-CrNiSiP clusters. The fact that vacancy clustering in Fe9Cr ferritic alloy resembles that of pure iron suggests that Cr solutes may play lesser role in irradiation hardening of ferritic alloys and steels than previously believed.

Keywords: Neutron irradiation, FeCr alloys and steels

1. Introduction

High Cr ferritic/martensitic (F/M) steels are candidate structural materials for the construction of key components in future reactors, since they offer better

*Corresponding author
Email address: mkonstan@sckcen.be (M.J. Konstantinović)

radiation resistance in comparison to austenitic steels [1, 2, 3, 4]. GenIV and fusion reactors will operate at temperatures well above 400 °C, with neutron doses foreseen to be in the range of 50 to 100 dpa [5, 6]. F/M steels are expected to be well suited to withstand these conditions, as they experience negligible swelling under neutron irradiation, offer good thermal conductivity and exhibit reduced thermal expansion. However, their potential use could be limited due to low temperature radiation embrittlement, which they experience when irradiated bellow 400 °C, even when the neutron dose is very low [7]. In search of minimal ductile-brittle transition temperature (DBTT) shift, the low temperature embrittlement behavior of F/M steels has been extensively studied as a function of the Cr content [8]. Accumulated results led to the empirical identification of the most optimal one to be at 9%Cr for reduced-activation F/M steels (T91, Eurofer97, F82H, HT9). From the modeling perspective, the minimum shift of DBTT at 9%Cr was largely ascribed to complex effects related with how Cr influences the microstructure evolution and redistributes itself under irradiation [9, 10]. In particular, the contribution of α' to increase strengthening above 9 %Cr has been clearly identified and estimated, in a 12 %Cr model alloy, to be likely to exceed 40% after neutron irradiation to about 0.6 dpa at about 300°C [11]. More difficult is to understand why should alloys become stronger for lower than 9% Cr content. A possible explanation in terms of different strength of $< 100 >$ versus $1/2< 111 >$ Cr decorated loops has been proposed in [10]; the different formation of voids depending on the ferritic versus ferritic/martensitic microstructure may also play a role [12]. In [10], based on atomistic simulations, it was also highlighted that α' precipitates are not especially strong obstacles to dislocation motion. Based on these data a full theoretical account of the role of Cr precipitates on hardening in high-Cr F/M model alloys and steels has been given in [13]. In this work, while recognizing that α' precipitates contribute significantly to hardening in 12%Cr alloys, it was also further confirmed that the inherent strength of α' precipitates is not especially high and that solute clusters may have a strength twice as high as Cr precipitates. Experimentally, however, in most cases it was difficult to separate and control different factors in order to deduce their individual contributions [14, 12]. It is therefore important to further study experimentally the role of minor alloying elements such as Ni, Si and P, as well as of the initial microstructure (e.g. ferritic versus martensitic) on the mechanical properties of F/M steels and alloys under irradiation.

With this aim in mind, the mechanical properties of neutron irradiated fully ferritic Fe-Cr ferritic model alloys, with minimal and similar C content, but with varying concentrations of Cr, Ni, Si and P, have been recently investigated together with actual 9%Cr F/M alloys [15]. The focus was on the effect on radiation hardening of the content of Cr and minor solutes such as Ni, Si and P, as well as on initial microstructure. Irrespective of irradiation temperature and of the Cr content, significant hardening was observed only in model alloys containing Ni, Si and P solute atoms, suggesting that Cr solutes play lesser role in irradiation hardening of F/M alloys steels than previously believed. The presence of minor solutes (Ni, Si, P) was found to be essential for the microstructural features that form under irradiation to have a hardening effect, i.e. to make the

features efficient obstacles to dislocation motion. These results were found to be in a very good agreement with previous atom probe tomography (APT) studies that have revealed that solute clusters containing not only Cr, but also minor solutes, form under neutron irradiation at 300 °C [16, 17]. Additionally, it was observed that the martensitic alloys harden much less than the ferritic ones. It is possible that the limited hardening is partly a consequence of higher dislocation density, specific grain structure or carbon distribution in comparison to ferrites, which would influence distribution of vacancies and self interstitials leading to the reduced formation of solute clusters.

The mechanism driving the formation of nano-sized solute rich clusters is currently under discussion, see [18] and references therein. The CrNiSiP clusters that form in lower density than e.g. α' precipitates in Fe-Cr alloys of any Cr content do not seem to correspond to any thermodynamic phase. Thus their origin should be rather attributed to radiation-induced segregation processes, in which point-defect catalyse the formation clusters that otherwise would not form. Importantly, the existence of a binding energy between typical minor solutes in Fe-Cr alloys and vacancies leads to their being dragged towards point-defect sinks [19], this being the likely mechanism of formation of solute-rich clusters [18]. Complexes that contain solute atoms and vacancies are stable because the binding with the vacancies provides the "glue" between solutes even in the absence of thermodynamic driving forces leading to phase separation via precipitation. Consequently, stable vacancy-solute clusters are expected to form, based on a radiation-induced precipitation mechanism. Similarly, some solutes such as specifically P and Cr are dragged by self-interstitials towards point-defect sinks [20], while self-interstitial clusters, similarly to vacancy clusters, exhibit binding energy with several solutes [21], so the formation of stable solute clusters by segregation of point-defect dragged solutes on point-defect clusters can be considered as a general mechanism, which suggests the association of solutes with point-defects. These are therefore the ingredients of an Object Kinetic Monte Carlo model used in this work to interpret and rationalize the experimental results.

In order to provide a solid interpretation of the mechanical property results that were reported in [15], and to verify for as much as possible the association between solutes and point-defects, a thorough microstructure examination is needed. In this study, the same neutron irradiated alloys that were previously mechanically tested are further investigated by positron annihilation spectroscopy (PAS) and small angle neutron scattering (SANS). The defect characterization based on these two techniques shows without any doubt that vacancy-CrNiSiP clusters do form and play a dominant role in irradiation hardening.

2. Materials, experiments and computation methods

2.1. Materials

Four ferritic and one F/M model alloys have been investigated in this study. Their chemical composition is given in Table 1. The Fe5Cr(NiSiP), Fe9Cr,

Table 1: The nominal composition of FeCr model alloys.

element (wt.%)	C	N	Si	P	S	Cr	Ni	Al	Fe
Fe9Cr FM	0.02	0.015	0.09	< 0.005	0.001	8.4	0.07	0.007	bal.
Fe9Cr	< 0.006	< 0.005	0.004	0.003	< 0.005	9.1	0.009	0.027	bal.
Fe9CrNiSiP	< 0.006	< 0.005	0.221	0.032	< 0.005	9.1	0.092	0.028	bal.
Fe5CrNiSiP	< 0.006	< 0.005	0.219	0.033	< 0.005	4.9	0.13	0.026	bal.
Fe14CrNiSiP	< 0.006	< 0.005	0.194	0.031	< 0.005	14.4	0.087	0.025	bal.

Fe9Cr(NiSiP) and Fe14Cr(NiSiP) alloys are all fully ferritic, with decreasing grain size ($\sim$ 30 to 100 micrometers) with increasing Cr and minor solute content, except in the case of the 14Cr [15] where the grain size is much larger. The Fe9Cr F/M alloy is essentially purely martensitic. Neutron irradiation was performed in the BR2 materials testing reactor of SCKCEN. Details on material fabrication and neutron irradiation were published elsewhere [15]. The microstructural investigation in this study has been performed on the samples that were irradiated at about 300 ^{0}C to neutron dose of 0.11 dpa.

2.2. PAS

Positron annihilation spectroscopy (PAS) experiments were performed with the Coincidence Doppler broadening spectrometer (CDB). The CDB spectra were measured using two Ge detectors. Details of the setup are described in [22]. CDB spectroscopy allows the measurement of the momentum distribution of the electron-positron pair and they are typically analyzed based on the S-parameter (line-shape parameter) and the W-parameter (wing parameter). The S and W-parameters are defined as the ratio of low momentum ($\mid p_L \mid < 2.5 \times 10^{-3} m_0 c$) and high momentum ($15 \times 10^{-3} m_0 c < \mid (p_L) \mid < 25 \times 10^{-3} m_0 c$) regions of the CDB spectra to the total momentum, respectively (where c is the speed of light and p_L is the longitudinal component of the positron-electron momentum along the direction of γ-ray emission). The annihilation of positrons with valence electrons contributes to the low momentum region (S-parameter), thus providing information about open volume defects. On the other hand, the annihilation of positrons with inner shell electrons contributes to the high-momentum region (W-parameter) and provides information about the chemical environment at the annihilation site.

2.3. SANS and Vickers hardness

The small angle neutron scattering (SANS) measurements were carried out at the instrument PAXY at LLB Saclay (France) [23]. Samples of 1 mm thickness were placed in a magnetic field of 1.5 T oriented perpendicular to the incident neutron beam of 0.5 nm wavelength. Two sample-detector distances of 2 and 6 m with corresponding collimation lengths were chosen, thus covering a range of scattering vector, Q, from 0.05 to 2.5 nm^{-1}. The raw data treatment including transmission measurement and correction for both background and detector sensitivity is described in [24]. For absolute calibration a standard sample

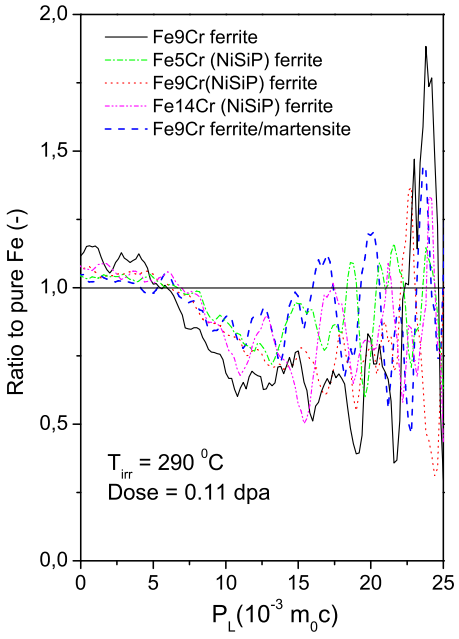

Figure 1: (Color online) Doppler broadening spectra of the FeCr alloys. Measurement error increases with P_L; minimum and maximum values are shown.

with known scattering cross section was used. Data analysis including separation of magnetic and nuclear scattering cross-sections was performed using the BerSANS software package [25]. The scattering cross-sections of the unirradiated reference samples were subtracted from the respective cross-sections of the irradiated samples in order to derive the characteristics of irradiation-induced scatterers. These difference scattering curves were transformed into size distributions of scatterers using an own code [26] based on the Monte Carlo method introduced by [27]. The volume fraction and number densities of scatterers in absolute units were obtained assuming non-magnetic scatterers (magnetic holes) in an Fe-9Cr matrix [28]. The A-ratio, A = 1 + M/N, was calculated from the magnetic (M) and nuclear (N) contributions of the scatterer. It is a one-parameter signature of the mean composition of irradiation-induced scatterers. A more detailed description about the A-ratio as function of the cluster composition is given in [29, 30].

Vickers hardness HV10 (load 98.1 N) was measured according to the standard DIN EN ISO 6507 using the unirradiated or irradiated SANS samples after the SANS experiments.

2.4. OKMC simulation

The Object Kinetic Monte Carlo (OKMC) model used in this study describes the evolution of an alloy under irradiation with stochastic events implementing

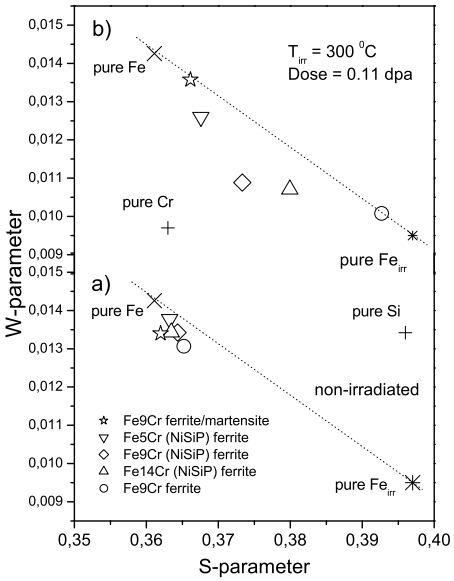

Figure 2: S versus W parameters of neutron irradiated FeCr alloys

the migration and interaction of diffusing species; these are point defects or complexes involving point defects and solutes, e.g., vacancy-solute clusters [18]. Key reactions in our OKMC model are the dragging of minor solute atoms by single point-defects, and the binding of solute atoms with small loops, which were parameterized based on DFT calculations [21]. In order to be applied to concentrated Fe-Cr alloys, the "grey alloy" approximation in the OKMC model was used for the chromium atoms, while all other minor alloying elements are included explicitly. The OKMC model within a "grey alloy" approximation, in which the effect of the alloying elements was translated into a change of the value of the parameters that define the mobility and stability of point defects and their clusters as a function of the nominal composition, has been previously successfully applied to reactor pressure vessel alloys [31, 32] and steels [33]. Thus, the OKMC model has been designed to describe the formation of vacancy clusters and NiSiP-rich clusters under irradiation, but cannot directly predict their Cr content, or the formation of α'-particles. This approximation is a compromise between the current capabilities of the OKMC technique and an explicit description of the formation of solute/point-defect clusters, which allows the results to be used for an assessment of the microstructural features that are expected to mainly cause radiation hardening.

3. Results and discussion

The CDB spectra of neutron-irradiated Fe-Cr alloys are shown in Fig.1. All irradiated materials exhibit an increase of the S-parameter and a decrease of the

W-parameter, indicating that positrons are trapped and annihilate at vacancy-rich complexes induced by neutron irradiation. Clearly, Fe9Cr ferrite has the strongest enhancement in the low momentum region of all materials. In the high momentum region, the smallest difference with respect to the reference Fe sample (represented by the dashed straight line) was observed for Fe9Cr FM alloy. The CDB spectra of all other alloys fall in between these two extreme cases. The properties of vacancy rich clusters in these alloys are further studied based on the W vs S parametric plot. The plot showing the W-parameter versus the S-parameter of both non-irradiated and neutron irradiated Fe-Cr alloys is presented in Fig.2, including the data for irradiated pure Fe [34]. This graph illustrates the evolution of vacancy-rich clusters after irradiation in various alloys. Non-irradiated alloys, Fig.2a, exhibit slightly higher the S-parameter and lower the W-parameter than pure Fe, mainly due to higher dislocation density in these alloys with respect of pure Fe.

The results of CDB measurements for materials which are neutron irradiated at 290 °C, in the form of the W-parameter versus the S-parameter, are given in Fig.2 b. After neutron irradiation, a significant increase of the S-parameter, as compared to non-irradiated materials, is observed for all alloys except Fe9Cr F/M. The largest increase of the S-parameter after neutron irradiation has been found for ferritic Fe9Cr. Overall, this is consistent with the known fact that ferrite develops more easily a void population than martensite [35]. This could indicate that the presence of Ni, Si and P solutes hinders the growth of vacancy clusters, by creating more stable and less mobile complexes, while Cr does not. This is consistent with the stronger interaction of these solutes with vacancies than Cr, as mentioned in the introduction [36]. Interestingly, the decrease of the W-parameter seems to be more than just the compensation to the increase of the S-parameter (narrowing of the CDB curve). In contrast to Fe9Cr and Fe9Cr F/M, the S- and W-parameters of Fe5,9,14Cr(NiSiP) do not lay on the straight line connecting pure Fe and neutron irradiated Fe points. W-S points in these three materials are displaced towards lower values of the W-parameter in comparison to W-S evolution of irradiated pure Fe. Since the W-parameter provides information about the chemical environment around annihilation site [37], these results are the signature of the formation of vacancy-solute clusters. Thus the experimental data confirms, at least in the case of vacancies, that solutes accumulate round point defect clusters.

The SANS spectra of Fe-Cr alloys are presented in Figs. 3 and 4. The magnetic SANS cross sections are presented in Fig.3 for ferritic Fe9Cr and Fe9Cr(NiSiP) alloys and in Fig.4 for the Fe9Cr F/M alloy; the Fe5,14Cr(NiSiP) alloys exhibit similar SANS spectra as the Fe9Cr(NiSiP), but are not shown to save space. Increased scattering intensities of the irradiated states are observed for the range Q $> 0.3nm^{-1}$ for all materials. The scattering intensity of the unirradiated condition of the ferrite/martensite alloy is 6 times higher than for the ferrite alloy at Q $= 0.3nm^{-1}$, and reach higher levels for Fe9Cr F/M than for all ferritic alloys. Obviously, this is due to differences in the microstructure between both types of alloys, which are unchanged during irradiation, for instance the existence of carbides.

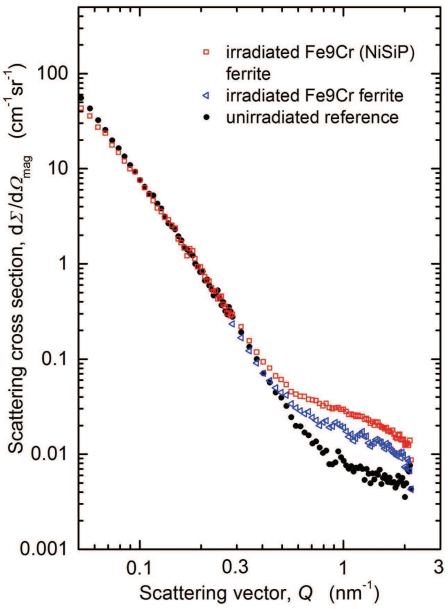

Figure 3: (Color online) Measured magnetic scattering cross-sections of pure Fe-9Cr, Fe9Cr (NiSiP) ferrite and unirradiated reference.

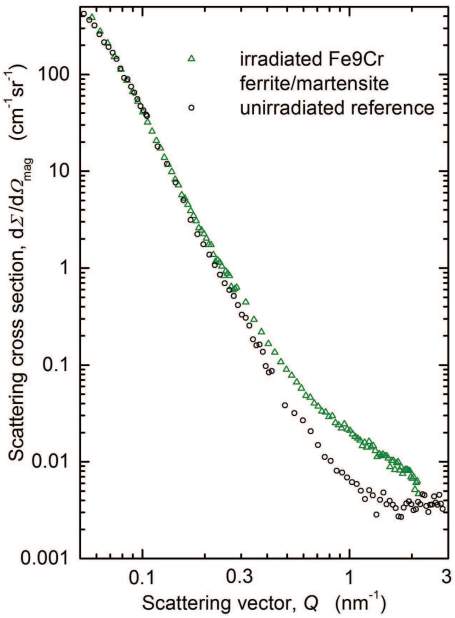

Figure 4: (Color online) Measured magnetic scattering cross sections of Fe9Cr ferrite/martensite and the unirradiated reference.

Table 2: Characteristics of irradiation-induced nano-features in Fe9Cr alloys irradiated up to 0.1 dpa derived by SANS (volume fraction c, number density N, mean radius R_{mean}, A-ratio), including the change of hardness value after irradiation Δ HV10)

material	c (vol %)	N ($\times 10^{16} cm^{-3}$)	R_{mean} (nm)	A-ratio	Δ HV10
Fe9CrC F/M	0.13 ± 0.01	19±4	1.04 ± 0.07	2.20 ± 0.2	27±3
Fe9Cr ferrite	0.15 ± 0.01	39±8	0.90 ± 0.02	1.45± 0.1	22±3
Fe9Cr(NiSiP) ferrite	0.29 ± 0.01	69±12	0.95 ± 0.05	1.90± 0.15	72±3
Fe5Cr(NiSiP) ferrite	0.13 ± 0.01	27±3	0.97 ± 0.08	3.50 ± 0.5	68±4
Fe14Cr(NiSiP) ferrite	1.75 ± 0.05	592±76	0.83 ± 0.03	2.15 ± 0.15	94±7

The estimated values of the A-ratio, volume fraction, number density and mean size are listed in Table 2. The nuclear scattering curves were found to exhibit similar shapes as the magnetic scattering curves, see [30] for Fe9Cr F/M. This indicates that nuclear and magnetic scatterers are the same objects - a prerequisite for the interpretation of the A-ratio in terms of composition. The A-ratio observed for ferritic pure Fe9Cr indicates that the majority of irradiation-induced scatterers are vacancy clusters. Indeed, vacancy clusters in Fe9Cr give rise to a theoretical A-ratio of 1.4 [30]. This observation is in an excellent agreement with the PAS data discussed above. The higher A-ratios of the other four alloys indicate a dominant contribution of solute clusters. It is worth to note that an A-ratio of 2.05 is expected for Cr-rich α'-phase particles [30], as observed in Fe14Cr(NiSiP). Moreover, the high volume fraction in Fe14Cr(NiSIP) provides additional argument for the presence of Cr-rich α'-phase particles in this alloy. However, if α'-particles were dominant in Fe9Cr(NiSiP) (A-ratio close to 2.05), they should also dominate in pure Fe9Cr, which is not the case. Therefore, it is reasonable to assume that the high A-ratio values in other three alloys are caused by other types of solute clusters, most probably vacancy-CrNiSiP solute clusters [16]. The difference between A-ratios of Fe5Cr(NiSiP) and Fe9Cr(NiSIP) probably indicate different chemical composition of vacancy-CrNiSiP solute clusters formed in these two alloys after neutron irradiation (e.g. different Cr content in the cluster) and/or different mixture with vacancies. Note that the PAS data exhibit higher value of the S-parameter in Fe9Cr(NiSiP) as compared to Fe5Cr(NiSiP), which could already explain the lower value of the A-parameter in Fe9Cr(NiSiP) in comparison to Fe5Cr(NiSiP). The size distributions are similar for all ferritic alloys.

Hardness measurements were performed on the same set of samples as those used for PAS and SANS measurements. The results are summarized in Table 2. Significant hardness after neutron irradiation has been observed only in the alloys containing minor solute elements, namely Fe5.9.14Cr(NiSIP), which is in an excellent agreement with tensile tests [15]. The mechanical properties of these alloys suggest, therefore, that Cr, even though present in large quantity in the alloy, as well as in the Cr-rich vacancy-NiSiP clusters, is not the main cause of hardening, probably with the only exception of when it contributes in the form of α' precipitates in the $14\%Cr$ alloy. In fact, the presence of minor

Table 3: Characteristics of irradiation-induced vacancy and solute clusters in FeCr alloys irradiated up to 0.11 dpa derived by OKMC (number density N and average size). Average size of the vacancy cluster is presented as the number of vacancies in a cluster D_{vac}, while the average size of the solute cluster is shown as their average cluster diameter R_{sol}.

material	$N_{vac}(\times 10^{17} cm^{-3})$	$D_{vac}(\#)$	$N_{sol}(\times 10^{16} cm^{-3})$	R_{sol} (nm)
Fe9CrC F/M	4.9	1.9	0	0
Fe9Cr ferrite	121	9.8	3.4	0.76
Fe9Cr(NiSiP) ferrite	34.0	2.0	48	0.93
Fe5Cr(NiSiP) ferrite	43.5	1.9	33	0.93
Fe14Cr(NiSiP) ferrite	37.1	2.1	34	0.94

solutes (Ni, Si, P) is essential for the microstructural features that form under irradiation to have a hardening effect, i.e. to make the features efficient obstacles to dislocation motion.

With this in mind, we performed OKMC simulation to calculate the properties of vacancy and solute clusters that are formed under neutron irradiation, in which chromium atoms are taken into account in a "grey alloy" approximation, so that the formation of vacancy-CrNiSiP solute clusters is governed mainly by the precipitation kinetics of Ni, Si and P. This assumption has been also supported by density functional theory [21], which predicts negligible binding energy of Cr to a vacancy. The OKMC results are summarized in Table 3. The "solute clusters" in Table 3 are defined as NiSiP solute atoms, independently of the content in point-defects. There are therefore 3 kinds of defects, all accounted for in the same statistics: (a) those with vacancies additionally to the NiSiP solutes; (b) those with self-interstitial atoms additionally to the NiSiP solutes; (c) those without point-defects but only NiSiP solutes. The presentation of our results in this way is consistent with the measurement performed by SANS, because all three categories of solute clusters as listed above are equally assimilated as "defects" without distinction of their vacancy or SIA defects contents. Likewise, the other category of defects as reported in Tab 3 are "vacancy clusters" as are seen by PAS: the reported number density includes both vacancy defects decorated by NiSiP solutes, and those not decorated by solutes. Even tough the OKMC calculation predicts a distribution of sizes of vacancy clusters to appear as a result of irradiation, the focus is here on the average values, since both PAS and SANS measurements provide only mean values.

The formation of large vacancy clusters with an average size of about 10 vacancy per cluster has been obtained for the Fe9Cr ferritic alloy. Clearly, this result is in full agreement with the PAS data, see Fig. 2, but it is mainly a consequence of the starting assumption that limits the role of chromium. Namely, Cr reduces the mobility of self-interstitial clusters with respect to pure Fe, without affecting the vacancy mobility. The reduced mobility of self-interstitial clusters enhances recombination with vacancies, leading to a vacancy population clusters slightly smaller than, but very similar to, the vacancy population in pure Fe. In contrast, the size of vacancy cluster is drastically reduced to just a few vacancies per cluster in all other alloys. Evidently, the presence of Ni, Si and P

solutes limits the growth of vacancy clusters in comparison to the Fe9Cr ferritic alloy, which leads to the decrease of the S-parameter in the PAS data. Small variations of the size of vacancy clusters in these alloys occurs due to the difference in minor solute concentrations, see Table 1. In contrast to ferritic alloys, the Fe9Cr F/M alloy has been modeled with higher sink strength than in the case of ferritic alloys (two orders of magnitude higher dislocation density and lower grain size). In this case, the OKMC model predicts a number density of vacancy clusters close to the non-irradiated case (note that no vacancy-solute cluster formation has been observed by OKMC in this alloy, see discussion below). However, vacancy clustering in Fe9Cr ferritic alloy irradiated to 0.11 dpa has limited effect on hardening, since the vacancy clusters are still to small to act as obstacles to dislocation motion. According to previous studies [12], significant effect of vacancy clustering on hardening in FeCr alloys is expected only at about 0.5 dpa and more.

The OKMC model calculation also provides information about the solute clusters. An average cluster size with a diameter of about 1 nm has been observed for all alloys, irrespectively of their chemical composition. These results are found to be in excellent agreement with the SANS results. Good quantitative agreement between the OKMC model and the SANS results has been also observed for what concerns the solute cluster number density, see Tables 2 and 3. In the case of neutron irradiation up to 0.11 dpa, a solute cluster number density of about 30 to 50 $\times 10^{16} cm^{-3}$ is expected in these alloys. The Fe9Cr ferritic alloy exhibits about 5 times lower solute cluster density than Fe9Cr(NiSiP), while no solute clusters were found in Fe9Cr F/M. In the Fe9Cr ferritic alloy, the growth of solute clusters is minimal because of the low concentration of minor solutes, while in Fe9Cr F/M no solute clusters are mainly the result of high sink strength. This effect is similar to the suppression of the growth of vacancy clusters. The solute number density calculated by the OKMC model in Fe5Cr(NiSiP) alloy has been observed to be slightly lower than in the case of Fe9Cr(NiSiP) and Fe14Cr(NiSiP). Most probably, this reduction occurs as a consequence of the variation in the mobility of self-interstitial clusters for different chromium concentrations, which is an integral part of the "grey" alloy approximation. This effect could potentially lead to the different solute cluster compositions that should show up in the values of the A-parameter. Indeed, the A-parameter of Fe5Cr(NiSIP) exhibits very different values in comparison to other alloys. However, the model is not detailed enough to allow an assessment of origin of the significantly higher A ratio that was measured in the case of the Fe5Cr(NiSIP) alloy. Finally, as expected, the OKMC model largely underestimate the solute cluster concentration in Fe14Cr(NiSiP) alloy, since it cannot predict the formation of α' particles.

Interestingly, despite the relatively low dose of 0.11 dpa, the number density of vacancy-solute clusters estimated by SANS and OKMC, see Tables 2 and 3 is comparable or even higher than in previous studies on similar alloys irradiated to higher dose [30, 16, 12, 38]. However, important differences existed in terms of composition and microstructure. For example, the Fe5Cr investigated in [38] contains no Ni and has low Si content, the latter being an element with strong

interaction with the vacancy [36], while the Fe5Cr(NiSiP) from [16, 30, 12] has large carbon content with ferritic/martensitic structure. Carbon is another element that strongly interacts with vacancies [39], which seems to be removed from the matrix in tempered martensite [12], while the martensitic structure offers more sinks for point-defects. The Fe5Cr(NiSIP) alloy investigated in this study, in contrast, has fully ferritic structure due to much lower carbon content, see Table 1. According to the findings in this study, therefore, the high number density of solute clusters in this class of alloys at low dose could be the consequence of the chemical composition (the content of minor solutes) and the microstructure (governed by the carbon content). Namely, the large ferritic grain size would favor the formation of vacancy clusters and the presence solutes that strongly interact with vacancies in the matrix, especially Si and P, would stabilize them, increasing their number.

Based on the details about the solute cluster composition, density and size deduced from the model, with numbers that agree with the experiment and help rationalize it, we conclude that the formation of solute clusters is crucial to induce the strengthening of the alloy, the Cr content being less important. Our model cannot predict the Cr content of solute clusters; likewise we do not know whether in the Fe9Cr ferritic alloy Cr accumulates around point-defect clusters or forms any type of agglomeration (the W parameter suggests no difference with respect to Fe). However, from the fact that no hardening is measured in Fe9Cr we should conclude that either Cr clustering does not occur or, if it does, its presence around point-defect clusters does not make them stronger obstacles as compared to Fe. It is possible that this occurs because, of all solutes, Cr is the one with the weakest binding with point defects [36, 21]. That is, the increase in radiation strengthening in Fe-Cr with respect to Fe that was formerly attributed to Cr [10] should be probably attributed to minor solutes, instead. This lack of Cr effect is more easily revealed in very low-carbon and high purity fully-ferritic materials, such as those used in the present work, than in alloys with largely martensitic, microstructure and/or of lesser purity, that were used in previous experiments. The effect of Cr redistribution and clustering on hardening becomes visible only when the formation of α' is suspected to occur, i.e. in the 14%Cr alloy. However, even when α' forms the contribution to hardening of solute clusters remains significant. As a matter of fact, even in alloys with higher Cr content than 9% and irradiated to higher dose where α' precipitates have clear hardening role [40, 41], the inclusion in the hardening equation of the effect of solute clusters is necessary. More to the point, separate analyzes of the data on Fe12Cr(NiSiP) showed that, for neutron irradiation of about 1 dpa, only roughly 30-40 % of the hardening could be attributed to α' precipitates [12], i.e. the same contribution as solute clusters, even tough the α' precipitate number density was more than one order of magnitude higher than that of CrNiSiP precipitates [30, 16], i.e. high densities of α' precipitates are needed to equal the contribution of solute clusters. Finally, it is noteworthy that in 9%Cr steels the role on hardening of clusters formed by minor solutes remains of crucial importance up to doses as high as 32 dpa [42]

4. Conclusions

PAS, SANS and hardness experiments were performed on neutron irradiated FeCr alloys. Hardness measurements were found to be in excellent agreement with the tensile test results published previously. They confirm the existence of irradiation hardening only in alloys containing minor solute elements. Moreover, both PAS and SANS experiments confirm in a consistent way the formation of large vacancy clusters in the Fe9Cr ferrite. In all ferritic alloys containing minor solutes, in contrast, vacancy-CrNiSIP clusters are clearly observed by both PAS and SANS experiments, thereby further confirming that solute clusters are associated with point-defect clusters. In PAS, the existence of vacancy-CrNiSIP clusters is manifested by the significant difference of the W-parameter with respect to those expected in both pure Fe or Fe9Cr alloys without minor solute elements. In SANS, their existence has been confirmed by the measurements of the defect volume fraction (number density) and the A-parameter. Most experimental microstructural results can be rationalized based on the OKMC model, which is implemented in a "grey alloy" approximation only for the chromium atoms, while all other alloying elements were included explicitly. This good agreement further suggests that solute clusters are formed by segregation of solutes at point-defect clusters, dragged there by single point-defects. Significant number of α' particles were observed in Fe14(NiSIP). However, while vacancy clusters and α'-precipitates contribute to hardening, their impact is less in comparison to the effect of solute clusters associated with point-defects.

Acknowledgements This work has received funding from the Euratom research and training programme 2014-2018 under grant agreement No. 755039 (M4F project). This work also contributes to the Joint Programme on Nuclear Materials (JPNM) of the European Energy Research Alliance (EERA).

5. Data availability

The raw/processed data required to reproduce these findings cannot be shared at this time as the data also forms part of an ongoing study.

References

[1] R.L. Klueh, D.R. Harris, High chromium ferritic martensitic steels for nuclear applications, ASTM (2001).

[2] R.L. Klueh, A.T. Nelson, J. Nucl. Mater. Ferritic steels for next-generation reactors, 371 (2007) 37-52.

[3] S. J. Zinkle, J. T. Busby, Structural materials for fission and fusion energy, Materials Today 12 (2009) 12.

[4] N. Singh, J.H. Evans, J. Nucl. Mater, Significant differences in defect accumulation behaviour between fcc and bcc crystals under cascade damage conditions, 226 (1995) 277-285.

[5] P. Yvon and F. Carré, Structural materials challenges for advanced reactor systems, J. Nucl. Mater. 385 (2009) 217-222.

[6] A. Zinkle, H. Muroga, S.J. Möslang, T. Tanigawa, Multimodal options for materials research to advance the basis for fusion energy in the ITER era, Nucl. Fusion, 53 (2013) 104024.

[7] Y. Chen, Irradiation effects of HT-9 martensitic steel, Nucl. Eng. and Technol. 45 (2013) 311.

[8] A. Kohyama, A. Hishinuma, D.S. Gelles, R.L. Klueh, W. Dietz, K. Ehrlich, Low-activation ferritic and martensitic steels for fusion application, J. Nucl. Mater. 233-237 (1996) 138-147.

[9] L. Malerba, G. Bonny, D. Terentyev, E.E. Zhurkin, M. Hou, K. Vörtler, K. Nordlund, Microchemical effects in irradiated Fe-Cr alloys as revealed by atomistic simulation, J. Nucl. Mater. 442 (2013) 486-498.

[10] D. Terentyev, G. Bonny, C. Domain, G. Monnet, L. Malerba, Mechanisms of radiation strengthening in FeCr alloys as revealed by atomistic studies, J. Nucl. Mater. 442 (2013) 470-485.

[11] F. Bergner, C.Pareige, M. Hernández-Mayoral, L. Malerba, C.Heintze, Application of a three-feature dispersed-barrier hardening model toneutron-irradiated FeCr model alloys, J. Nucl. Mater. 448 (2014) 96-102.

[12] M.J. Konstantinović, W. Van Renterghem, M. Matijašević, B. Minov, M. Lambrecht, T. Toyama. M. Chiapetto and L. Malerba, Mechanical and microstructural properties of neutron irradiated FeCrC alloys, Phys. Status Solidi (A), 213 (2016) 2988-2994.

[13] G. Monnet, Multiscale modeling of irradiation hardening: Application to important nuclear materials, J. Nucl. Mater. 508 (2018) 609-627.

[14] M. Matijašević and A. Almazouzi, Effect of Cr on the mechanical properties and microstructure of FeCr model alloys after n-irradiation, J. Nucl. Mater. 377 (2008) 147-154.

[15] M.J. Konstantinović, M. Lorenzo, Mechanical properties of FeCr alloys after neutron irradiation, J. Nucl. Mater. 528 (2020) 151879.

[16] V. Kuksenko, C. Pareige, C. Genevois, F. Cuvilly, M. Roussel, P. Pareige, Effect of neutron-irradiation on the microstructure of a Fe12at.%Cr alloy, J. Nucl. Mater. 415 (2011) 61-66.

[17] B. Gómez-Ferrer, C. Heintze, C. Pareige, On the role of Ni, Si and P on the nanostructural evolution of FeCr alloys under irradiation, J. Nucl. Mater. 517 (2019) 35-44.

[18] N. Castin, G. Bonny, A. Bakaev, F. Bergner, C. Domain, J.M. Hyde, L. Messina, B. Radiguet and L. Malerba, The dominating mechanisms for the formation of solute-rich clusters in steels under irradiation, arXiv:1912.06828 [cond-mat.mtrl-sci].

[19] L. Messina, M. Nastar, N. Sandberg, P. Olsson, Systematic electronic-structure investigation of substitutional impurity diffusion and flux coupling in bcc iron, Phys. Rev. B 93 (2016) 184302.

[20] L. Messina, T. Schuler, M. Nastar, M.-C. Marinica, P. Olsson, Solute diffusion by self-interstitial defects and radiation-induced segregation in ferritic Fe-X (X=Cr, Cu, Mn, Ni, P, Si) dilute alloys, Acta Mat. 191 (2020) 166-185.

[21] C. Domain, C.S. Becquart, Solute $< 111 >$ interstitial loop interaction in α-Fe: A DFT study, J. Nucl. Mater. 499 (2018) 582-594.

[22] K. Verheyen, M. Jardin, A. Almazouzi, Coincidence Doppler broadening spectroscopy in Fe, FeC and FeCu after neutron irradiation, J. Nucl. Mater. 351 (2006) 209-215.

[23] http://www-llb.cea.fr/fr-en/pdf/paxy-llb.pdf

[24] P. Strunz, J. Saroun, U. Keiderling, A. Wiedenmann, R. Przenioslo, General formula for determination of cross-section from measured SANS intensities, J. Appl. Cryst. 33 (2000) 829-833.

[25] U. Keiderling, The new 'BerSANS-PC' software for reduction and treatment of small angle neutron scattering data, Appl. Phys. A 74 (2002) S1455-1457.

[26] A. Wagner, F. Bergner, A. Ulbricht, C.D. Dewhurst, Small-angle neutron scattering of low-Cu RPV steels neutron-irradiated at 255 °C and post-irradiation annealed at 290 °C, J. Nucl. Mater. 441 (2013) 487-492.

[27] S. Martelli, P.E. Di Nunzio, Particle Size Distribution of Nanospheres by Monte Carlo Fitting of Small Angle X-Ray Scattering Curves, Part. Part. Syst. Charact. 19 (2002) 247e255.

[28] S. Mühlbauer, D. Honecker, É. A. Périgo, F. Bergner, S. Disch, A. Heinemann, S. Erokhin, D. Berkov, C. Leighton, M. R. Eskildsen, A. Michels, Magnetic small-angle neutron scattering, Rev. Mod. Phys. 91 (2019) 015004 pp75.

[29] A. Ulbricht, F. Bergner, J. Böhmert, M. Valo, M.-H. Mathon, A. Heinemann, SANS response of VVER440-type weld material after irradiation, post-irradiation annealing and reirradiation, Phil. Mag. 87 (2007) 1855-1870.

[30] C. Heintze, F. Bergner, A. Ulbricht, H. Eckerlebe, The microstructure of neutron-irradiated Fe-Cr alloys: A small-angle scattering study, J. Nucl. Mater. 409 (2011) 106-111.

[31] M. Chiapetto, L. Malerba, C.S. Becquart, Nanostructure evolution under irradiation in FeMnNi alloys: A "grey alloy" object kinetic Monte Carlo model, J. Nucl. Mater. 462 (2015) 91-99.

[32] M. Chiapetto, C.S. Becquart, C. Domain, L. Malerba, Nanostructure evolution under irradiation of Fe(C)MnNi model alloys for reactor pressure vessel steels, Nucl. Instrum. Methods Phys. Res. B 352 (2015) 56-60.

[33] M.J. Konstantinović, I. Uytdenhouwen, G. Bonny, N. Castin, L. Malerba and P. Efsing, Radiation induced solute clustering in high-Ni reactor pressure vessel steel, Acta Mat. 179 (2019) 183-189.

[34] M. Lambrecht, L. Malerba, A. Almazouzi, Influence of different chemical elements on irradiation-induced hardening embrittlement of RPV steels, J. Nucl. Mater. 378 (2008) 282.

[35] V. Bryk, O. Borodin, A. Kalchenko, V. Voyevodin, V. Ageev, A. Nikitina, V. Novikov, V. Inozemtsev, A. Zeman, F. Garner, in: proceedings of the 11th International Topical Meeting on Nuclear Applications of Accelerators, AccApp 2013, Bruges, Belgium, (2013).

[36] P. Olsson, T. P. C. Klaver and C. Domain, *Ab initio* study of solute transition-metal interactions with point defects in bcc Fe, Phys. Rev. B 81 (2010) 054102.

[37] Y. Nagai, M. Hasegawa, Z. Tang, A. Hempel, Y. Kawazoe, A. Kawai, F. Kano, Positron confinement in ultrafine embedded particles: Quantum-dot-like state in an Fe-Cu alloy, Phys. Rev. B 61 (2000) 6574-6578.

[38] M. Bachhav, L. Yao, G. R. Odette, E. A. Marquis, Microstructural changes in a neutron-irradiated Fe6 at.%Cr alloy J. Nucl. Mater. 453 (2014) 334-339.

[39] M. J. Konstantinović and L. Malerba, Dissolution of carbon-vacancy complexes in Fe-C alloys, Phys. Rev. Mat. 1 (2017) 053602.

[40] M. Bachhav, G. R. Odette b, E. A. Marquis, Microstructural changes in a neutron-irradiated Fe15 at.%Cr alloy, J. Nucl. Mater. 454 (2014) 381-386.

[41] D. Bhattacharyya, T. Yamamoto, P. Wells, E. Marquis, M. Bachhav, Y. Wu, J.Davis, A.Xu, G. Robert Odette, Microstructural changes and their effect on hardening in neutron irradiated Fe-Cr alloys, J. Nucl. Mater. 519 (2019) 274-286.

[42] B. Gómez-Ferrer, C. Dethloff, E. Gaganidze, L. Malerba, C. Hatzoglou, C. Pareige, Nano-hardening features in high-dose neutron irradiated Eurofer97 revealed by atom-probe tomography, J. Nucl. Mater. 537 (2020) 152228.